

Statistical mechanics of collisionless orbits. III. Comparison with N-body simulations

Liliya L. R. Williams¹, Jens Hjorth² and Radosław Wojtak^{2,3}

ABSTRACT

We compare the DARKexp differential energy distribution, $N(\varepsilon) \propto \exp(\phi_0 - \varepsilon) - 1$, obtained from statistical mechanical considerations, to the results of N-body simulations of dark matter halos. We first demonstrate that if DARKexp halos had anisotropic velocity distributions similar to those of N-body simulated halos, their density and energy distributions could not be distinguished from those of isotropic DARKexp halos. We next carry out the comparison in two ways, using (1) the actual energy distribution extracted from simulations, and (2) N-body fitting formula for the density distribution as well as $N(E)$ computed from the density using the isotropic Eddington formula. Both the methods independently agree that DARKexp $N(E)$ with $\phi_0 \approx 4 - 5$ is an excellent match to N-body $N(E)$. Our results suggest (but do not prove) that statistical mechanical principles of maximum entropy can be used to explain the equilibrated final product of N-body simulations.

1. Introduction

In this series of papers we revisit the use of statistical mechanics to address the structure of self-gravitating N-body systems, such as dark matter halos. In Hjorth & Williams (2010; Paper I) we showed that if it is correct to think of finite self-gravitating collisionless isotropic systems as the most probable configuration in the energy state space, then their energy distribution is given by a truncated exponential differential energy distribution, DARKexp; $N(\varepsilon) \propto \exp(\phi_0 - \varepsilon) - 1$, where ε and ϕ_0 are dimensionless energy and potential depth, respectively. The resulting structures have central density cusps.

In Williams & Hjorth (2010; Paper II) we used the Extended Secondary Infall Model (ESIM) to confirm that restricted dynamical evolution can drive a system to the DARKexp state. ESIM largely fulfills the stipulations imposed by DARKexp; it is spherically symmetric, and its dynamics make

¹Department of Astronomy, University of Minnesota, 116 Church Street SE, Minneapolis, MN 55455; llrw@astro.umn.edu

²Dark Cosmology Centre, Niels Bohr Institute, University of Copenhagen, Juliane Maries Vej 30, DK-2100 Copenhagen Ø, Denmark; jens@dark-cosmology.dk

³Nicolaus Copernicus Astronomical Center, Bartycka 18, 00-716 Warsaw, Poland; wojtak@camk.edu.pl

for efficient energy redistribution among particles, but does not allow the redistribution of angular momentum, which is not addressed in deriving DARKexp. ESIM generates a wide range of potential depths, as quantified by DARKexp’s sole parameter, ϕ_0 . ESIM halos are not exactly isotropic, many show radial anisotropy, and some have tangential anisotropies. The anisotropy profiles vary between halos. These variations appear to be random; with no consistency, or ‘universality’ between halos.

In contrast, N-body halos do show well defined anisotropy, which appears to be as universal as the density profile (Hansen & Moore 2006; Hansen et al. 2010). The halo centers are isotropic but the outer parts have significant radial anisotropy. It is not surprising that N-body and ESIM halos have different anisotropy characteristics. ESIM dynamics include radial forces and accelerations, but no tangential accelerations (only velocities). Simulations, on the other hand, operate in full three dimensions, so tangential forces can redistribute particles’ angular momenta and establish a universal anisotropy profile. Therefore it is possible that the presence of the well defined, universal anisotropy profile of N-body halos indicates an important element of the equilibrium structure of simulated halos, not accounted for in DARKexp models.

A full theory for the distribution of particles in energy-angular momentum space using the maximum entropy principle is yet to be developed. In the meantime, we ask if we can limit ourselves to comparing energy distributions only, without regard to non-zero anisotropy. Since whatever produces the anisotropy profile in simulated halos may also effect the energy distribution, it is not immediately obvious that DARKexp $N(E)$ can be compared to that of N-body halos. To proceed one must first determine what influence the anisotropy has on DARKexp $N(E)$ and density profile. If the anisotropy of N-body halos is such that it has no effect on $N(E)$ and $\rho(r)$, then one can compare the DARKexp and N-body $N(E)$ without worrying that anisotropy—and by implication whatever physics is present in simulations but was neglected in deriving DARKexp—will invalidate the comparison.

In Section 2 we show that if anisotropy is similar to what the N-body simulations produce, then $N(E)$ and $\rho(r)$ are unchanged compared to their isotropic counterparts. Therefore we argue that a comparison between DARKexp and N-body $N(E)$ can be justifiably made, and carry it out in two ways, as described in Sections 3.1 and 3.2.

2. $N(E, L)$ distributions of DARKexp models

2.1. Generating self-consistent sets of $N(E, L)$, $\rho(r)$ and $\beta(r)$

A geometrically spherically symmetric non-rotating system is fully described by the distribution of its particles in the two dimensional plane of energy, E and angular momentum, L ; $N(E, L)$. The range of energies is bounded on one end by the value of the deepest central potential, and the escape energy, $E = 0$ on the other end. For every E there is a maximum L which corresponds to the circular orbit at that energy; $L_{max}(E)$ is an upper envelope in the (E, L) plane. The lower

boundary is $L = 0$, implying a radial orbit. An example of an L vs. E plot and the $L_{max}(E)$ envelope can be found in Wojtak et al. (2008), for the particular case of numerically generated universal halos.

Even though the $N(E, L)$ distribution contains all the information about a system, there is no simple relation (that we know of) between it and the corresponding density and anisotropy profiles.

For the purposes of this work we need to check if a set of $N(E, L)$, $\rho(r)$, and anisotropy distributions is self-consistent (Sections 2.3 and 2.4), or, generate self-consistent sets of these distributions (Section 2.5). Anisotropy is defined as usual, $\beta(r) = 1 - \frac{\sigma_\theta^2(r)}{\sigma_r^2(r)}$; in spherical systems the two tangential velocity dispersions are equal, $\sigma_\theta = \sigma_\phi$. We use the following procedure. Given input distributions $N(E, L)$ and $\rho(r)$ we numerically generate a halo by drawing particles from the $N(E, L)$ distribution and adding up, or superimposing their orbits. The orbit superposition is done as follows. The system's potential $\Phi(r)$ is calculated from the input density profile. For each particle picked randomly from $N(E, L)$ we find its radial velocity, $v_{rad}(r)$, and apo- and peri-centers using the energy equation, $E = \Phi(r) + \frac{1}{2} [v_{tan}^2(r) + v_{rad}^2(r)]$, where the angular momentum is related to the radially dependent tangential velocity through $v_{tan}(r) = L/r$. The density that a particular particle contributes at a given radius is proportional to the amount of time it spends there, i.e., $\propto v_{rad}^{-1} dr / \int_{r_{peri}}^{r_{apo}} v_{rad}^{-1} dr$. Thus a halo is built up from its individual particles. If the density profile generated in this fashion matches the input $\rho(r)$, then the set of $\rho(r)$ and $\beta(r)$ (computed afterward from the radial and tangential velocity dispersions) represent a self-consistent solution for the input $N(E, L)$.

In this work, the only input energy distributions and density profiles we use are those of the isotropic DARKexp models. In Sections 2.3 and 2.4 we use the above procedure to determine if specific L -distributions are consistent with DARKexp. In Section 2.5 we seek, through trial-and-error, an L -distribution that produces a specific anisotropy profile. So, if for a given L -distribution the input $\rho(r)$ and the output $\rho(r)$ from orbit superposition do not match then the L -distribution is rejected. (Note that acceptance/rejection is not done on individual particle basis; only whole halos are accepted or rejected.) The procedure is repeated until an acceptable L -distribution is found.

This method has some features in common with the Schwarzschild orbit superposition method (Schwarzschild 1979), where a self-consistent equilibrium halo is built up from its constituent orbits. There is no dynamical evolution.

2.2. Anisotropy and the distribution of L

To generate halos, one needs an input $N(E, L)$. While DARKexp gives us the distribution in E , it says nothing about how orbits should be distributed in L to produce a given $\beta(r)$. To guide us, we start with some well known results connecting the energy distribution and the distribution

function, f . In general,

$$N(E, L) dE dL = 8\pi^2 L f(E, L) T_r(E, L) dE dL, \quad (1)$$

where T_r is the radial period of orbits (for example, see Appendix A of Wojtak et al. (2008)). For isotropic systems, $f = f(E)$. Hénon (1959) proved that only three types of potentials have T_r that depends on E alone: the point mass, the uniform density sphere, and the isochrone potential (see also Efthymiopoulos et al. (2007)). It is then more instructive to write eq. 1 as

$$N(E, L^2) dE dL^2 = 4\pi^2 f(E) T_r(E) dE dL^2. \quad (2)$$

The right hand side—and hence the left hand side—has no explicit L -dependence, therefore the number of orbits at a given E , between two L values is proportional to dL^2 , which means that for these three potentials isotropy implies a uniform distribution in L^2 .

With this result in mind, one can rewrite eq. 1 to describe systems where orbits are distributed uniformly in L^δ ,

$$N(E, L^\delta) dE dL^\delta = \frac{8\pi^2}{\delta} L^{2-\delta} f T_r dE dL^\delta. \quad (3)$$

If the distribution in a given parameter is uniform, that means the function has no explicit dependence on it. In the case of eq. 3, the expression for $N(E, L^\delta)$ has no explicit L^δ , or L dependence. Further assuming $T_r = T_r(E)$, implies that $L^{2-\delta} f \equiv h(E)$ is a function of E only, and hence f is separable; $f = h(E)L^{\delta-2}$. These are systems of constant anisotropy, $\beta = 1 - \delta/2$ (Hénon 1973). A $\beta = 0$ system is recovered for $\delta = 2$. Even though T_r is not strictly a function of E only for a general system, it appears to be a very good approximation for many potentials. Hence a uniform distribution in L^δ can be used to approximate constant β systems of arbitrary density profiles.

2.3. Isotropic halos

In this section we generate $N(E, L)$ distributions for isotropic DARKexp models. Although we know from Hénon (1959) that a strictly uniform distribution in L^δ with $\delta = 2$ cannot produce isotropic systems for DARKexp, we nevertheless try a uniform distribution of particles in L^2 . This is shown as black points in the left panel of Figure 1, for DARKexp $\phi_0 = 4$. The magenta curve represents the upper boundary, $L_{max}(E)$. We apply the orbit superposition procedure described above, with an isotropic DARKexp $N(E)$ and $\rho(r)$ as the input, shown as dashed black curves in the top panel of Figure 2. The resulting density profiles are shown as the red, magenta and blue solid lines for $\phi_0 = 2, 4, 8$ DARKexp models, respectively. These agree very well with the input $\rho(r)$, making this a self-consistent set of isotropic DARKexp halos.

We conclude that isotropic DARKexp halos (with DARKexp form for the $N(E)$) are very well described by a uniform orbit distribution in L^δ , where $\delta = 2$. The deviations from this, which we know have to be present, appear to be smaller than the precision required in the present paper.

2.4. Anisotropic halos; $\beta \approx 0.5$

For comparison, in the right panel of Figure 1 we show the case where, for any given E , the distribution is uniform in L , i.e. $\delta = 1$, so by the arguments of Section 2.2 these systems should have (nearly) constant $\beta = 0.5$. The anisotropy profiles of the orbit superposition halos are presented in the bottom panel of Figure 3 as the red, magenta and blue solid curves for $\phi_0 = 2, 4, 8$ DARKexp models, respectively. They do, in fact, have $\beta \approx 0.5$.

The DARKexp input density profiles are the as black dashed lines in the top panel, while the orbit superposition profiles are represented by red, magenta and blue lines. These do not match the input $\rho(r)$, and therefore DARKexp $N(E)$, which we used as the input energy distribution, is not consistent with constant anisotropy as large as $\beta = 0.5$.

A comment is in order. Inspection of Figure 3 shows that the systems obtained by orbit superposition obey the anisotropy-density inequality introduced by An & Evans (2006) for the central halo regions, and extended to apply to all radii by Ciotti & Morganti (2010). It states that $\gamma \geq 2\beta$ (recall that $\rho(r) \propto r^{-\gamma(r)}$). Applied to our systems it means that if $\beta = 0.5$, the density slope cannot be shallower than $\gamma = 1$ anywhere in the system. This slope is represented by a dotted line segment in the upper panel of Figure 3. Our three density profiles are steeper than this at all radii. As a consequence of the anisotropy-density inequality, the oscillations in the density slope (Paper II) are erased, and the asymptotic slope is attained at much larger radii than in the isotropic models.

2.5. Anisotropic halos; $\beta(r) \approx \beta_{\text{N-body sim}}(r)$

Here we repeat the orbit superposition procedure but aim to generate anisotropy profiles similar to those of N-body simulated halos. Since these are not constant, a uniform distribution in L^δ will not work. Through trial and error we came up with a Gaussian distribution in L^2 . The full distribution in the E vs. L^2 plane is,

$$N(\epsilon, L^2) d\epsilon dL^2 \propto N(\epsilon) \times \exp \left\{ - \left([L^2/L_{max}^2(\epsilon)] - \left[\frac{a_1}{a_2(\epsilon/\phi_0)} + a_2 \right] \right)^2 / (2a_3) \right\} d\epsilon dL^2, \quad (4)$$

where $N(\epsilon) \propto \exp(\phi_0 - \epsilon) - 1$ is the DARKexp form. As in Papers I and II we use dimensionless energy and potential, $\epsilon = \beta_T E$, and $\phi_0 = \beta_T \Phi_0$, where Φ_0 is the system's potential depth, and β_T is its (negative) inverse temperature. The constants (a_1, a_2, a_3) are $(0.25, 1.00, 0.20)$ for $\phi_0 = 2$, $(0.25, 0.75, 0.15)$ for $\phi_0 = 4$, and $(0.25, 0.50, 0.10)$ for $\phi_0 = 8$.

The density and anisotropy profiles are shown as red, magenta and blue solid lines in the two panels of Figure 4. The anisotropy profiles generated through orbit superposition (red, magenta and blue curves in the bottom panel) are quite close in shape to the universal anisotropy profile. The latter is plotted (dotted line) using the Einasto profile $\gamma = 2(r/r_{-2})^\alpha$ with $\alpha = 0.17$ (Navarro et al. 2004) combined with the anisotropy-density slope relation, $\gamma = -0.8 - 5\beta$ (Hansen et al.

2010). The thick portion of the dotted line represents the region where the $\gamma - \beta$ relation can be trusted (Navarro et al. 2010).

Each of the three orbit superposition density profiles (red, magenta, blue) matches its corresponding isotropic DARKexp profile (dashed black) very closely, which means that DARKexp $N(E)$ remains a good description for systems with anisotropies as large as those seen in simulations of universal halos. In other words, DARKexp $N(E)$ and density profiles originally derived for isotropic systems, are also consistent with systems whose $\beta(r)$ profiles are isotropic at the center and radially anisotropic closer to virial radii. We conclude that we can compare DARKexp $N(E)$ to that of N-body simulated halos, and safely ignore the anisotropy of the latter.

3. Comparing DARKexp $N(E)$ to that of simulated halos

Having demonstrated that universal anisotropy is too small to have an effect on $N(E)$ we now compare the DARKexp energy distribution to that of simulated universal halos, using two methods, described below.

3.1. Using $N(E)$ of simulated halos

Here we determine the differential energy distribution of dark matter particles residing inside the virial sphere of simulated halos. For this purpose we use a sample of 36 cluster-size relaxed halos extracted from a $z = 0$ snapshot of a N -body simulation of a standard Λ CDM cosmological model (for details of the simulation and the halo catalogue see Wojtak et al. 2008). This halo sample has already been used for calculating the distribution function and testing its phenomenological model with radially changing anisotropy (Wojtak et al. 2008). Each halo contains from 5×10^5 to 5×10^6 particles inside its virial sphere defined in terms of the mean overdensity, $\langle \rho \rangle / \rho_c \approx 100$, where ρ_c is the present critical density.

We calculate $N(E)$ for each halo independently by counting particles in energy bins. Then we combine all profiles into one and evaluate the median profile and the dispersion within the halo sample (blue curve and light blue area in Figure 5). To combine the halos, we scale the binding energies by $V_s^2 = GM(< r_{-2})/r_{-2}$ and the particle numbers by $N(< r_{-2})$, where r_{-2} is the radius where $\gamma(r_{-2}) = 2$. These scalings preserve scale-free similarities of the phase-space properties of halos including the differential energy distribution itself. They also diminish the differences between $N(E)$ profiles of individual halos with varying virial masses and scale radii. The scale radii, r_{-2} , were obtained by fitting the NFW profile to the density profiles of simulated halos. We emphasize that the results are independent of the assumption of a fitting formula and remain the same if the scale radii are calculated by finding a maximum of $\rho(r)r^2$, which is a fitting-independent method of measuring r_{-2} .

Although our analysis is restricted to the virialized parts of halos, we expect to encounter particle populations which are not fully equilibrated, e.g., particles which have only recently entered the virial sphere. In order to separate the energy range of these particles we indicate in Figure 5 the value of the gravitational potential at the virial radius r_v of all halos (see the black line and light gray rectangle showing the median value and the 1σ scatter within the halo sample). All relative energies, $\Phi_0 - E$, below this value are covered by particles moving along the orbits confined inside the virial sphere so that this energy range likely represents a fully equilibrated particle population. On the other hand, the upper energy range is partially populated by orbits extending beyond the virial sphere so that it likely includes a particle population which has not settled to equilibrium. It is worth noting that at the energy separating these two energy regimes, i.e., $E \approx \Phi(r_v)$, $N(E)$ starts deviating from an exponential growth predicted by the DARKexp model. At less bound energies, $E > \Phi(r_v)$, the presence of unequilibrated particle population manifests itself in an exponential cut-off of $N(E)$.

We fitted the median profile of $N(E)$ for N -body halos with the DARKexp model given by $N/N_0 = \exp[-\beta_T(E - \Phi_0)] - 1$, parametrized by the normalization N_0 and the inverse temperature β_T . The fitting was restricted to the energy range associated with the fully equilibrated particle population, i.e., $\Phi_0 - E \lesssim 3V_s^2$ (see Figure 5). It yields $\beta_T = 0.91 V_s^2$, which leads to the dimensionless potential depth of the halos $\phi_0 = 4.6$. This best fit ϕ_0 is consistent with the most favourable range of values resulting from comparing DARKexp model with the best analytical approximations of the universal density profile ($\phi_0 \approx 4 - 5$; Section 3.2). Given this agreement in ϕ_0 , and the results in Figure 5 we conclude that the DARKexp fit (dashed magenta curve) is a very good match to the $N(E)$ profile from simulations.

3.2. Using $\rho(r)$ fitted to simulated halos

Several fitting formulae have been suggested to describe the density profiles of N -body halos. The original double power-law NFW form was introduced by Navarro et al. (1997) as the universal shape for cold dark matter halos. It was later pointed out that simulated halos are even better fit with Einasto profiles (Navarro et al. 2004; Merritt et al. 2006). The S&M profile (Stadel et al. 2009) was recently proposed as a very good fit to the inner most regions, $r \lesssim r_{-2}$.

As in Paper II, one can compare the density profiles of numerically generated halos to those of isotropic DARKexp models. In Figure 6 we plot the density slope γ vs. the log of the radius. The original NFW fitting formula (short-dash black curve) is fairly similar to DARKexp (three solid black curves). The Einasto profile (short-long-dash red straight line) tracks DARKexp considerably better than NFW, and does so for more than three decades in radius. While the Einasto is a straight line in the figure, DARKexp is ‘concave’, i.e., its density slope changes less rapidly with increasing radius. The S&M profile (long-dash blue curve) also has some concavity, and in this sense, it curves to mimic the DARKexp in the inner halo region. It is interesting to note that as the successive fitting formulae become better descriptors of the N -body halos (NFW \rightarrow Einasto \rightarrow

S&M) they also get closer to the shape of the DARKexp density profile.

Since DARKexp ($\phi_0 \approx 4 - 5$) and N-body density profiles are very similar, and we already showed in Section 2.5 that anisotropy can be ignored for our limited purposes, we can assume isotropy and obtain $N(E)$ from the density fitting functions of N-body simulations. From $\rho(r)$ we first calculate $f(E)$, using the isotropic Eddington formula, and then $N(E)$ ¹.

The results are shown in Figure 7 for five Einasto profiles (solid blue curves), parametrized by the α index of Navarro et al. (2004); α between 0.07 and 0.27, in steps of 0.05. In calculating these we used 7 radial decades of $\rho(r)$ between $10^{-5} r_{-2}$ and $100 r_{-2}$, which contain most of the systems' mass. We then fitted Einasto $N(E)$ with the DARKexp form, $N/N_0 = \exp[-\beta_T(E - \Phi_0)] - 1$. The fitting yields N_0 and β_T . As before, the product $\beta_T \Phi_0$ is the dimensionless potential depth ϕ_0 , the only shape parameter in DARKexp.

In Figure 7 the DARKexp fits are represented by dashed magenta curves, and the best fit ϕ_0 are indicated in the plot. Among these five cases the best match occurs at $\alpha \approx 0.17$, which is also the average of halos simulated by Navarro et al. (2004). For $\alpha \lesssim 0.1$ the two distributions do not fit at all; and, perhaps not coincidentally, such α values are not encountered in simulations.

4. Conclusions

It is often said that $N(E)$ is primarily determined by $\rho(r)$, and visa versa (Binney & Tremaine 1987; Merritt et al. 1989), and that $\beta(r)$ has very little effect on this. We have quantified this statement for the specific case of DARKexp $N(E)$ and $\rho(r)$. We find that if DARKexp halos had $\beta(r)$ shapes similar to those of N-body simulated halos, their density and energy distributions could not be distinguished from those of isotropic DARKexp halos. This means that even without a full theory of collisionless equilibrium $N(E, L)$, which would presumably explain $\beta(r)$ of simulated halos, one can compare the DARKexp and N-body $N(E)$, while ignoring non-zero anisotropy. We have carried out this comparison in two ways, using (1) the actual energy distribution extracted from simulations, and (2) N-body $\rho(r)$ fitting functions, and $N(E)$ computed from $\rho(r)$ using the isotropic Eddington formula. Both of these methods agree that DARKexp $N(E)$ with $\phi_0 \approx 4 - 5$ is an excellent match to N-body $N(E)$. This suggests that statistical mechanical principles of maximum entropy can be used to explain the equilibrated final product of N-body simulations. In the future we will extend the maximum entropy principle used to derive DARKexp to include L . This will hopefully explain $\beta(r)$ observed in simulated halos.

¹ One might be tempted to use the isotropic Jeans equation, thereby obtaining the velocity dispersion profile $\sigma(r)$, and then estimating kinetic energy as $\frac{1}{2}\sigma^2$. Combining this with the potential gives E for particles at that radius. This procedure will give wrong results because the velocity distribution function (VDF) is implicitly assumed to be Maxwellian, which is wrong. The importance of VDF and its deviations from Maxwellian was discussed in Kazantzidis et al. (2004) and Hansen (2009).

The Dark Cosmology Centre is funded by the Danish National Research Foundation. LLRW would like to thank the hospitality of the Dark Cosmology Centre and the University of Zürich where part of this work was carried out. The authors are grateful to Stefan Gottlöber, who kindly agreed for one of his CLUES simulations, (<http://www.clues-project.org/simulations.html>) to be used in this paper. The simulation has been performed at the Leibniz Rechenzentrum (LRZ) Munich.

REFERENCES

- An, J. H. & Evans, N. W. 2006. *ApJ*, 642, 752
- Binney, J. & Tremaine, S. 1987, *Galactic Dynamics*, Princeton University Press, 1st edition
- Ciotti, L. & Lucia Morganti, L. 2010, Preprint, arXiv:1006.2344.
- Efthymiopoulos, C., Voglis, N. & Kalapotharakos, C. 2007, in *Topics in Gravitational Dynamics*, Lecture Notes in Physics, Vol 729, Springer Berlin/Heidelberg. (Link: <http://www.springerlink.com/content/3401462523t3076h>)
- Hansen, S. H., Juncher, D. & Sparre, M. 2010, Preprint, arXiv:1005.1643
- Hansen, S. H. 2009, 694, 1250
- Hansen, S. H. & Moore, B. 2006, *NewA*, 11, 333
- Hénon, M. 1959, *Ann. d’Astrophys.* 22, 126
- Hénon, M. 1973, *A&A.* 24, 229
- Hjorth, J. & Williams, L. L. R. 2010, *ApJ*, in press (Paper I)
- Kazantzidis, S., Magorrian, J. & Moore, B. 2004, *ApJ*, 601, 37
- Merritt, D., Tremaine, S. & Johnstone, D. 1989, *MNRAS*, 236, 829
- Merritt, D., Graham, A. W., Moore, B., Diemand, J., & Terzic, B. 2006, *AJ*, 132, 2685
- Navarro, J. F., Frenk, C. S. & White, S. D. M. 1997, *ApJ*, 490, 493
- Navarro, J. F. et al. 2004, *MNRAS*, 349, 1039
- Navarro, J. F. et al. 2010, *MNRAS*, 402, 21
- Schwarzschild, M. 1979, *ApJ*, 232, 236
- Stadel, J., Potter, D., Moore, B., Diemand, J., Madau, P., Zemp, M., Kuhlen, M. & Quilis, V. 2009, *MNRAS*, 398, L21

Williams, L. L. R. & Hjorth, J. 2010, ApJ, in press (Paper II)

Wojtak, R., Lokas, E. L., Mamon, G. A., Gottloeber, S., Klypin, A. & Hoffman, Y. 2008, MNRAS, 388, 815

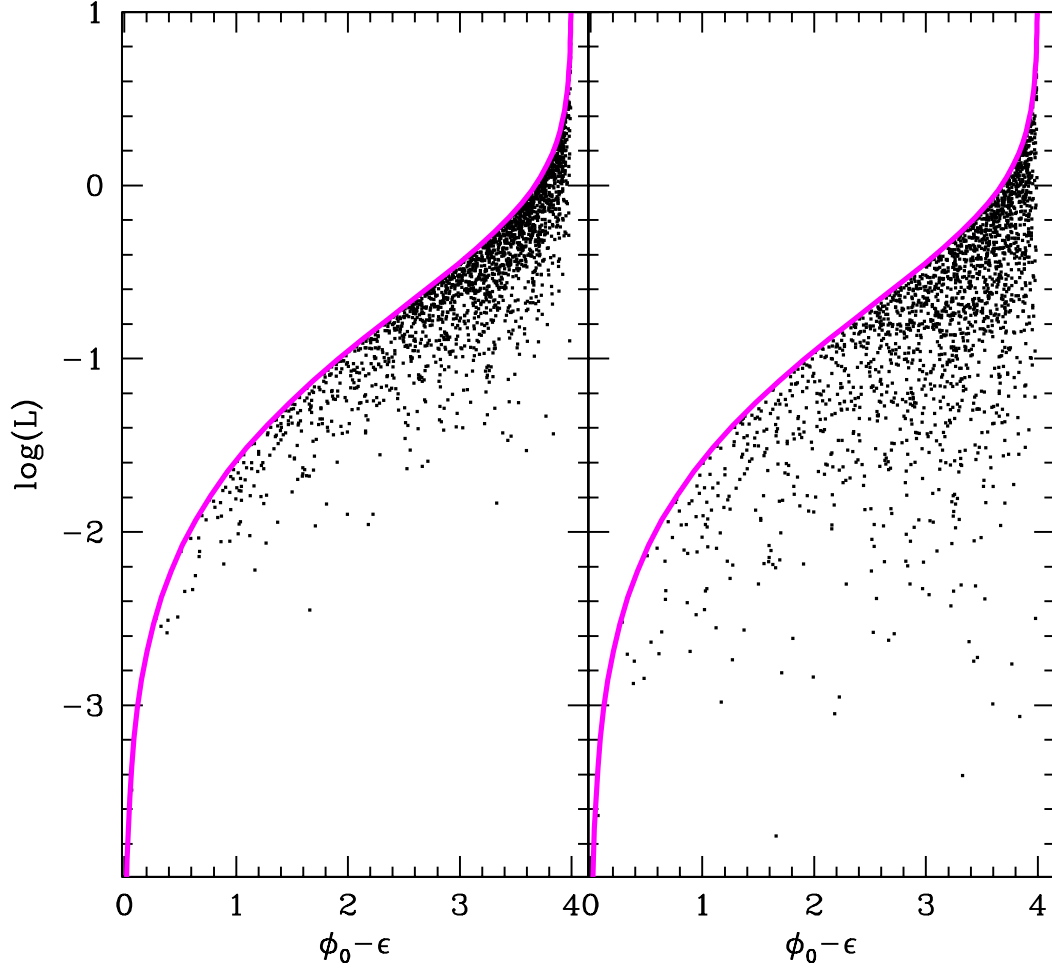


Fig. 1.— The log of angular momentum vs. the energy of particles making up halos. The energy distribution is the DARKexp $N(\varepsilon)$, with $\phi_0 = 4$ and particles shown are a realization of this distribution. The magenta line is the envelope corresponding to circular orbits, $L_{max}(E)$. *Left panel:* For a given E , the distribution in L^2 is uniform between 0 and $L_{max}^2(E)$. This gives an approximately isotropic system (Section 2.2; Figure 2). *Right panel:* For a given E , the distribution in L is uniform between 0 and $L_{max}(E)$. This gives constant $\beta(r) \approx 0.5$ (Section 2.2; Figure 3).

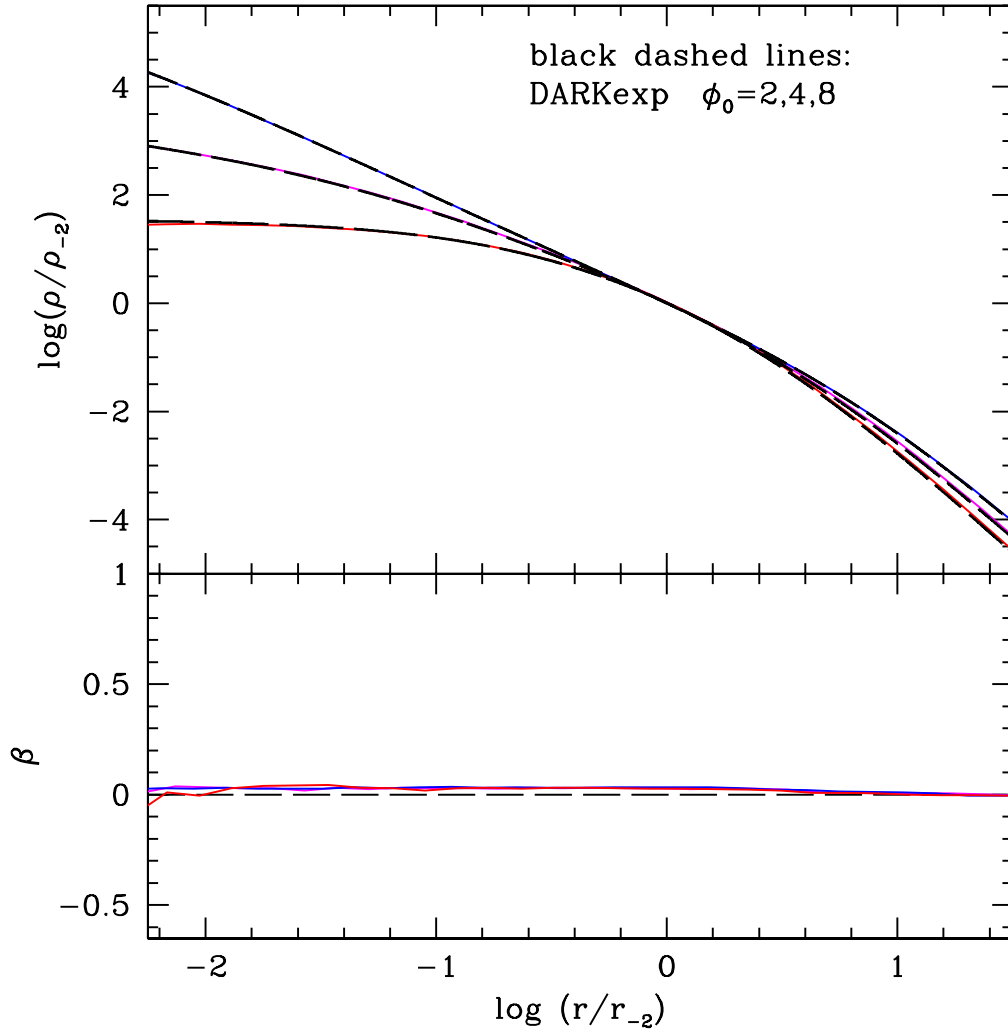


Fig. 2.— Density and anisotropy profiles for DARKexp models (dashed black curves), and halos generated using the method described in Section 2.1 (solid color curves). To achieve isotropy for the red, magenta, and blue solid curve halos we used a uniform distribution in L^2 , illustrated in the left panel of Figure 1.

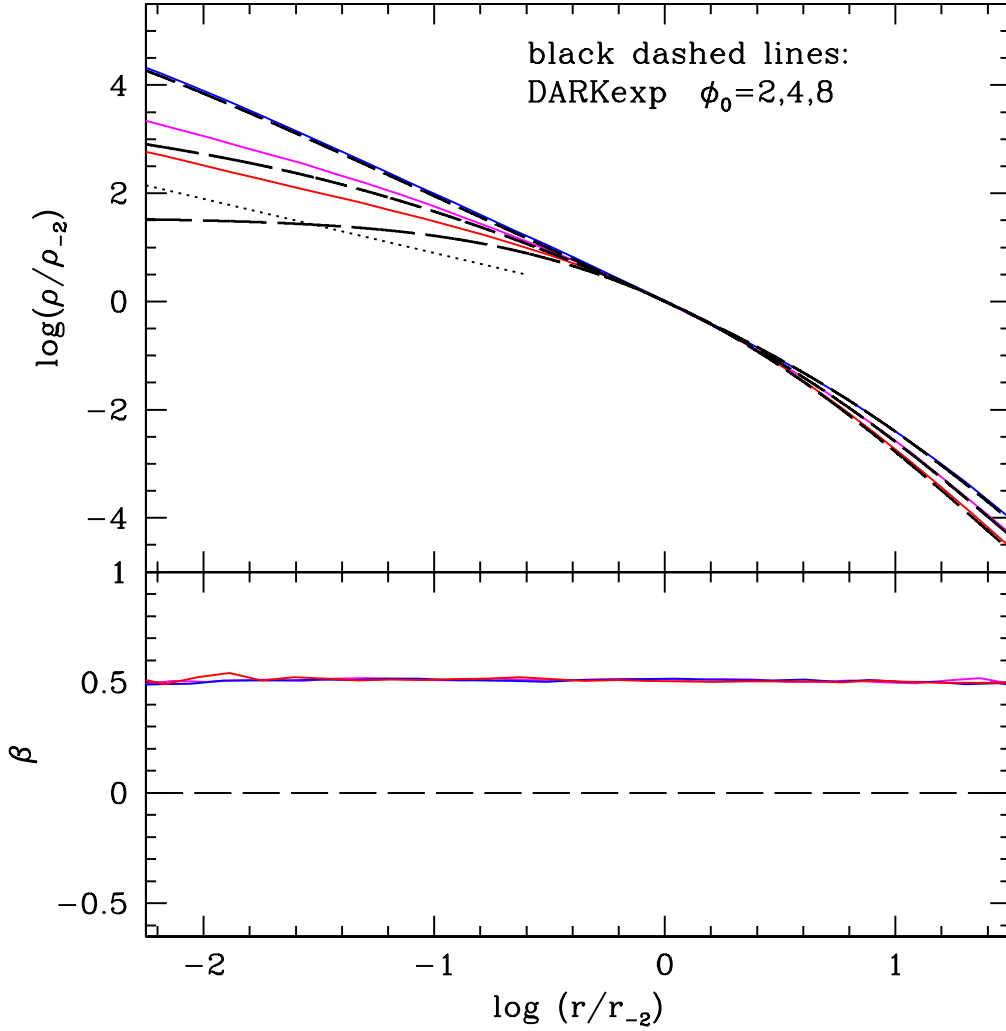


Fig. 3.— Density and anisotropy profiles for DARKexp models (dashed black curves), and halos generated using the method described in Section 2.1 (solid color curves). At every E , the distribution in L is uniform between 0 and $L_{max}(E)$; this distribution is illustrated in the right panel of Figure 1, and produces halos with $\beta \approx 0.5$. These systems obey the density-anisotropy relation, $\gamma \geq 2\beta$ since the density slope is never shallower than $\gamma = 1$, shown as the thin dotted line segment in the upper panel.

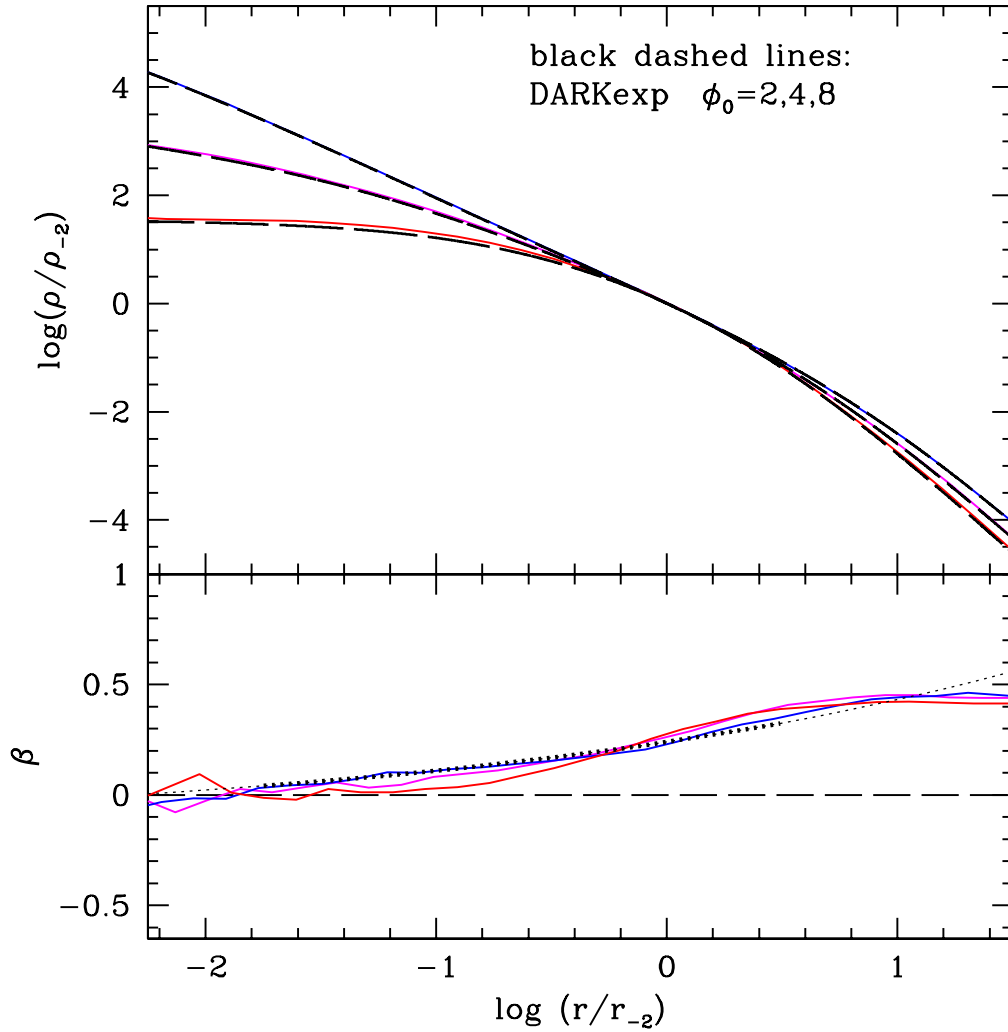


Fig. 4.— Density and anisotropy profiles for DARKexp models (dashed black curves), and halos generated using the orbit superposition method described in Section 2.1. These density profiles (red, magenta, and blue curves) agree very well with the isotropic DARKexp $\rho(r)$. The distribution in the L vs. E plane (see Section 2.5) was chosen such that the anisotropy profile would look similar to that of N-body halos. The latter is plotted (dotted line) using the Einasto profile $\gamma = 2(r/r_{-2})^\alpha$ with $\alpha = 0.17$ (Navarro et al. 2004) combined with the anisotropy-slope relation, $\gamma = -0.8 - 5\beta$ (Hansen et al. 2010). The thick portion of the dotted line represents the region where the $\gamma - \beta$ relation can be trusted.

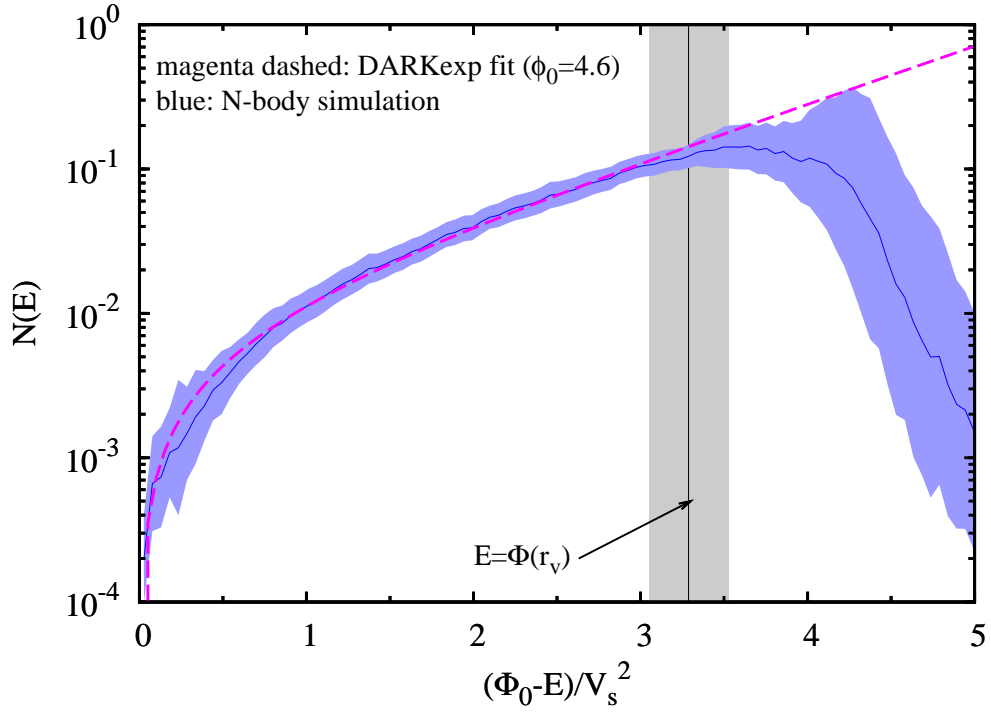


Fig. 5.— Comparison between $N(E)$ from N -body simulation (blue curve) and the DARKexp fit with $\phi_0 = 4.6$ (dashed magenta curve). The blue curve and light blue area represent the median profile and the 1σ scatter within the halo sample. The light gray area indicates the gravitational potential at the virial sphere (with the width corresponding to the 1σ scatter within the halo sample and the black line showing the median value). It defines an upper limit of the relative energy for a set of particle orbits which are fully confined inside the virial sphere.

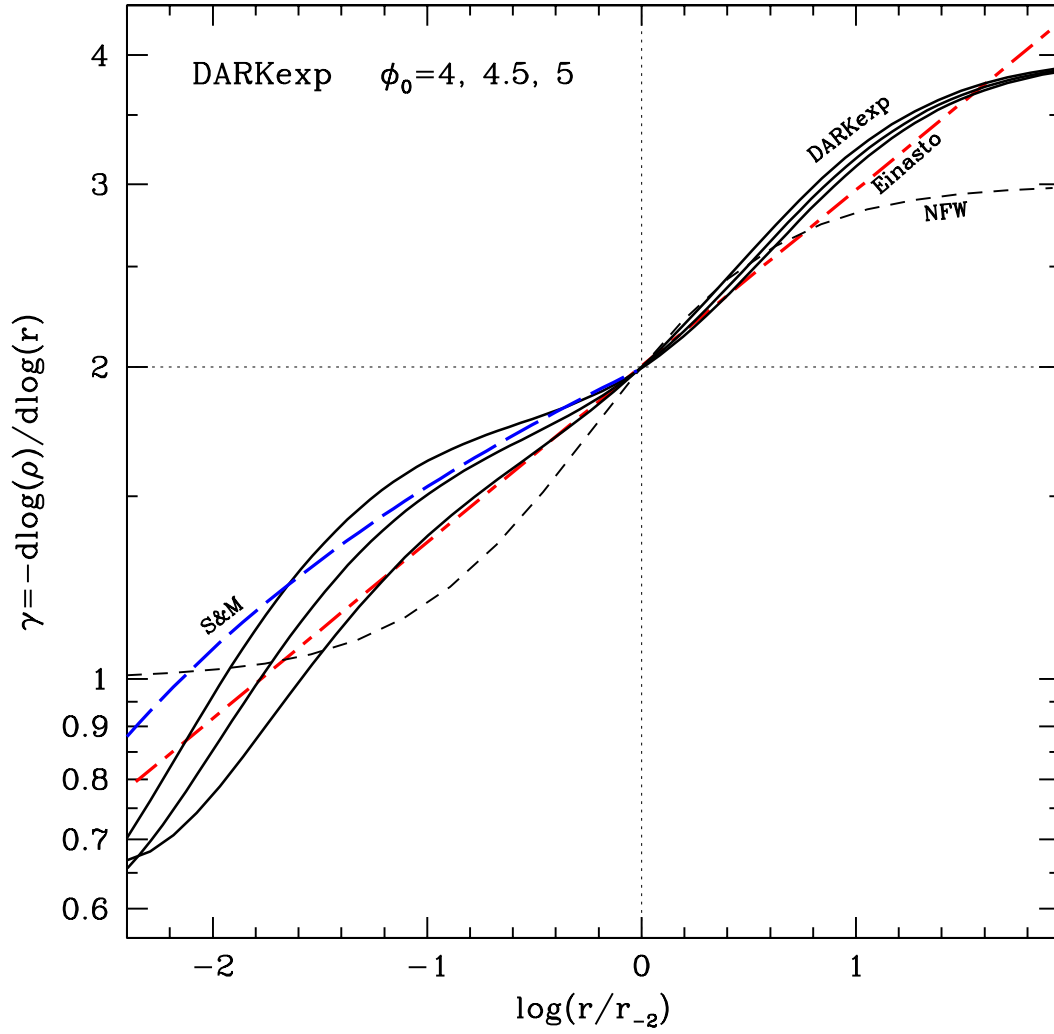


Fig. 6.— Comparison of DARKexp density profile slopes (three solid black curves) with N-body fitting functions: Einasto (Navarro et al. (2004) $\alpha = 0.17$, short-long-dash red straight line), NFW (short-dash black curve), and S&M (Stadel et al. (2009); long-dash blue curve). The last profile is meant to fit only the inner region of N-body halos, so the radial range outside of r_{-2} is not plotted.

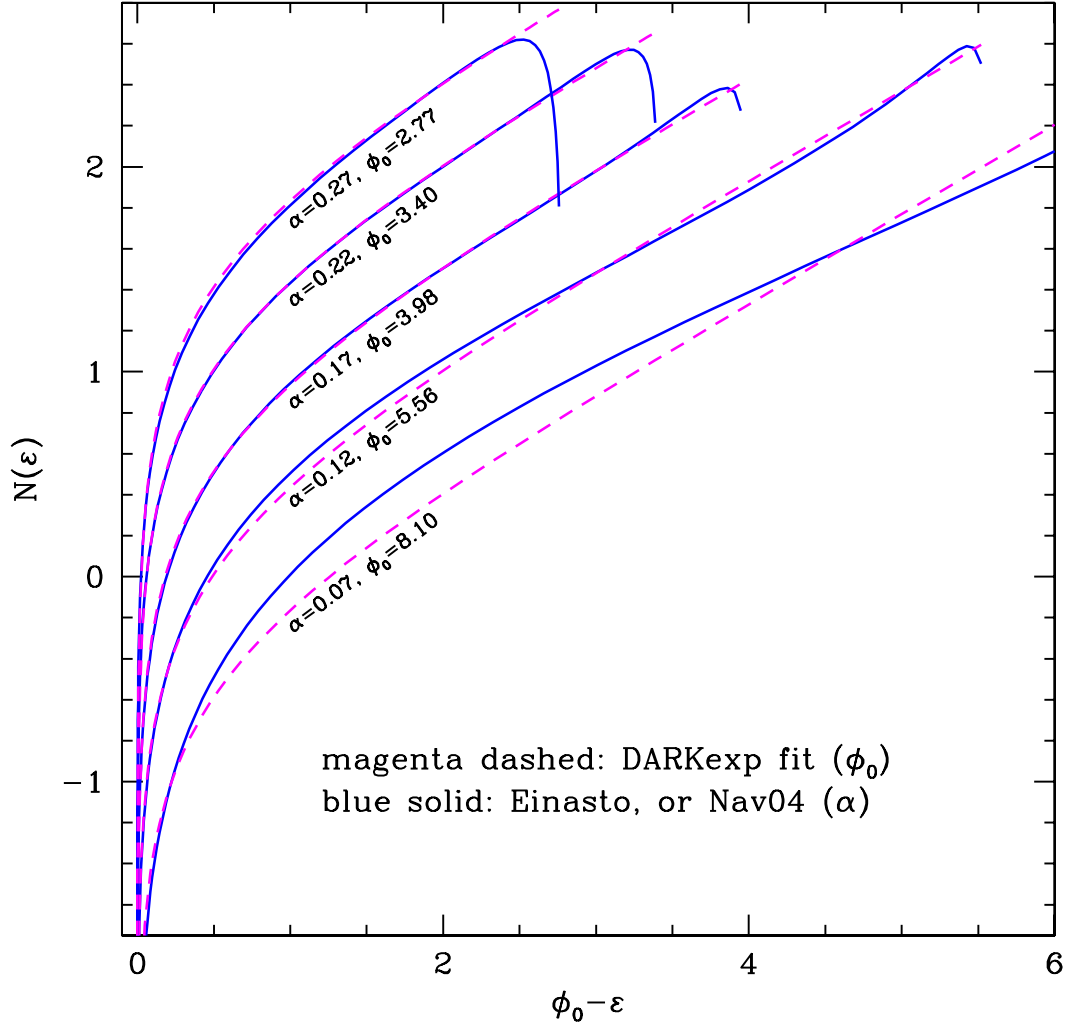


Fig. 7.— Comparison between $N(E)$ for DArkexp and N-body halos; see Section 3.2. A range of Einasto profiles (solid blue), with $\alpha = 0.07, 0.12, 0.17, 0.22, 0.27$ were fit with DArkexp (dashed magenta), and the fitted ϕ_0 values are shown in the plot. The best match occurs for the α value (≈ 0.17) which happens to be the average of simulated halos (Navarro et al. 2004). For $\alpha \lesssim 0.1$ the two distributions do not fit at all, and these α values are not encountered in simulations.